

Geophysical Research Letters

RESEARCH LETTER

10.1029/2020GL091918

Key Points:

- The importance of storm direction in peak flow distribution is mainly driven by the relative difference of storm and watershed size
- Expected changes in predominant storm trajectories can significantly modify peak flow distributions
- Regionalization of peak flow distributions should account for the effects of the relative orientation of storms and watersheds

Supporting Information:

Supporting Information may be found in the online version of this article.

Correspondence to:

G. Perez,
gabriel.perez.mesa@vanderbilt.edu

Citation:

Perez, G., Gomez-Velez, J. D., Mantilla, R., Wright, D. B., & Li, Z. (2021). The effect of storm direction on flood frequency analysis. *Geophysical Research Letters*, 48, e2020GL091918. <https://doi.org/10.1029/2020GL091918>

Received 30 NOV 2020

Accepted 24 APR 2021

The Effect of Storm Direction on Flood Frequency Analysis

G. Perez¹ , J. D. Gomez-Velez^{1,2} , R. Mantilla³ , D. B. Wright⁴ , and Z. Li⁴

¹Department of Civil and Environmental Engineering, Vanderbilt University, Nashville, TN, USA, ²Department of Earth and Environmental Science, Vanderbilt University, Nashville, TN, USA, ³Department of Civil and Environmental Engineering, IIHR – Hydroscience & Engineering, The University of Iowa, Iowa City, IA, USA, ⁴Department of Civil and Environmental Engineering, University of Wisconsin-Madison, Madison, WI, USA

Abstract Storm direction modulates a hydrograph's magnitude and duration, thus having a potentially large effect on local flood risk. However, how changes in the preferential storm direction affect the probability distribution of peak flows remains unknown. We address this question with a novel Monte Carlo approach where stochastically transposed storms drive hydrologic simulations over medium and mesoscale watersheds in the Midwestern United States. Systematic rotations of these watersheds are used to emulate changes in the preferential storm direction. We found that the peak flow distribution impacts are scale-dependent, with larger changes observed in the mesoscale watershed than in the medium-scale watershed. We attribute this to the high diversity of storm patterns and the storms' scale relative to watershed size. This study highlights the potential of the proposed stochastic framework to address fundamental questions about hydrologic extremes when our ability to observe these events in nature is hindered by technical constraints and short time records.

Plain Language Summary Estimating the likelihood of extreme events such as floods is becoming more challenging because climate change affects storm patterns worldwide. This study focuses on understanding how storm direction affects the probability distribution of peak flows, which is essential for floodplain mapping and engineering design of resilient infrastructure under future climate. Our results suggest that storm direction has minor implications for these probability distributions in medium-sized watersheds or smaller (order of 4,000 km²) but can significantly affect larger watersheds, particularly for the largest flood events. Our findings point to avenues for future interdisciplinary analyses of the complex, dynamic role of rainfall structure in flooding.

1. Introduction

Flood frequency analysis (FFA)—estimating the probability distribution of peak flows—is a common practice in hydrology. It plays a central role in engineering design, floodplain mapping, river restoration, and the assessment of ecosystem services along river corridors (Hansh, 2012). Over the last century, we have seen significant theoretical and computational advances in FFA; however, fundamental challenges remain due to the scarcity of peak flow observations (Perez, Mantilla, Krajewski, & Wright, 2019; Stedinger & Griffis, 2008) and the lack of a consistent framework that accounts for hydrologic nonstationarity due to natural and anthropogenic changes in land use and climate (Hirabayashi et al., 2013; Milly et al., 2014).

Multiple hydrologic drivers and physical processes modulate peak flows, including the spatiotemporal variability of rainfall, antecedent soil moisture conditions, hydraulic channel properties, and river network topology and geometry. In particular, previous efforts have shown that *storm direction*, defined as the dominant direction of the moving rainstorm as it traverses the domain of interest, significantly affects the magnitude of individual peak flow events (e.g., Volpi et al., 2013). The role of storm direction in shaping peak flow distributions, however, remains unexplored, and its potential importance can be gleaned from two distinct perspectives: The impact of climate change on storm tracks and the estimation of peak flow distributions using so-called “regionalized” techniques (Dawdy et al., 2012).

Regarding the change of storm tracks in a changing climate, previous efforts to examine potential changes in flood frequency under future climate projections have primarily focused on rainfall frequency and intensity (e.g., Cheng & AghaKouchak, 2015), with no attention to how storm direction changes may alter

peak flow response statistics. Global circulation models suggest that atmospheric circulation changes will increase atmospheric water vapor and cause a poleward shift in storm tracks (Mbengue & Schneider, 2013; Tamarin-Brodsky & Kaspi, 2017). However, it remains unknown how atmospheric circulation changes will affect the local and regional trajectories of extreme storms, prompting calls for further research (W. Chang et al., 2016). A recent empirical characterization of historical changes in storm direction across the contiguous United States found that a large fraction of the eastern United States has seen a clockwise trend in the dominant direction of precipitation potentially associated with climate variability (Goodwell, 2020). The ubiquitous nature of these trends emphasizes the importance of a mechanical perspective to understand the potential implications for FFA.

From the perspective of hydrologic regionalization, widely used regional flood frequency analysis (RFFA) methods pool peak streamflow data from gauging stations to estimate peak flow distributions at gauged and ungauged locations within a region of interest (Hamed & Rao, 2019). RFFA uses regression analysis to estimate peak flows as a function of hydrogeomorphic predictors, typically in upstream watershed areas alone (e.g., Perez et al., 2018b). These regression models are trained and validated with data from gauged locations within a “homogeneous region” that has sufficiently similar climatologic and hydrologic characteristics to justify the “pooling” of stations (Eash et al., 2013; Hosking & Wallis, 1993). The definition of this homogeneous region does not consider the watershed orientation relative to the predominant storm tracks. Therefore, RFFA implicitly assumes that peak flow distributions are unaffected by storm direction even though adjacent watersheds can significantly differ in orientation within a region with similar preferential storm patterns (see Figures S1 and S2).

From a mechanistic perspective, the role of storm direction in runoff generation has been explored with laboratory experiments (de Lima & Singh, 2003) and rainfall-runoff modeling in natural and synthetic watersheds (C.-L. Chang, 2007; Han et al., 2004; Kim & Seo, 2013; Seo & Schmidt, 2013, 2014) forced by real (Lee et al., 2015; Sigaroodi & Chen, 2016; ten Veldhuis et al., 2017) and synthetic (Fang et al., 2019; Gao & Fang, 2019; Nunes et al., 2006) storms. In general, the importance of storm direction in the peak flow response depends on the compounding effects of rainfall (e.g., storm extent, speed, duration, and intensity; Marco & Valdés, 1998; Singh, 2005) and watershed (e.g., geometry and river network structure) characteristics (Ayalew & Krajewski, 2017; Perez et al., 2018a). Based on these studies, the relationship between peak flow response and storm properties can be summarized in the following conclusions: (1) The effect of storm direction increases when the storm size is significantly smaller than the watershed size, and (2) the peak flow response tends to increase when the storm travels downstream along the main channel (Gao & Fang, 2019; Volpi et al., 2013).

This mechanistic understanding has not been translated into FFA and estimates of peak flow probability distributions. This issue is particularly challenging because peak flow probability distributions encapsulate a spectrum of rainfall-runoff events forced by storms of varying characteristics (Furey et al., 2016; Perez, Mantilla, Krajewski, & Quintero, 2019) that can result in different levels of sensitivity to storm direction. Furthermore, the extent to which the potential spectrum of storm characteristics and watershed response are represented in instrumental records is difficult to determine. With this in mind, this study uses a novel framework that combines physics-based hydrologic simulations with large numbers of stochastically generated rainfall events to derive flood frequency distributions under varying preferential storm directions for two watersheds. This analysis is then used to identify the role of storm direction in flood frequency and its implications for regionalization approaches.

2. Methods

We consider two unregulated watersheds within the central agricultural region of Iowa, U.S. (Figure 1). These include the medium-scale Turkey River (TR) watershed with a drainage area of 4,385 km² and the mesoscale Cedar River (CR) watershed with a drainage area of 20,168 km². The drainage area difference allows us to simultaneously evaluate the role of storm direction and scale in peak flow probability distributions.

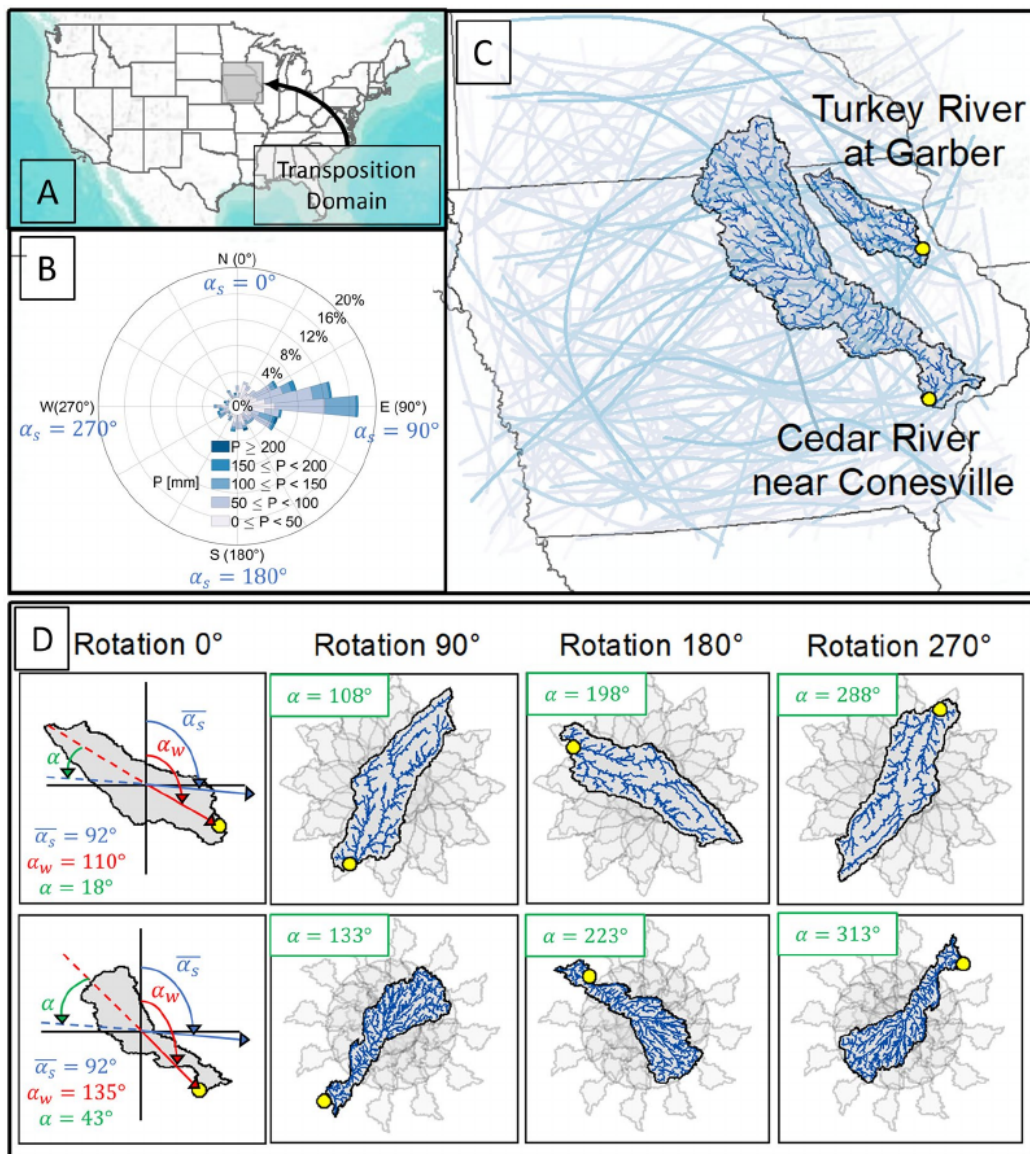


Figure 1. Panel a shows the transposition domain used in RainyDay. The rose plot in panel b represents the number of storms that are traveling to a specific direction over the transposition domain used in RainyDay and discretized by the watershed's rainfall accumulation (colors). The blue lines in panel c represent individual parent storm trajectories detected using the algorithm TITAN. Panel d shows four examples of watershed rotations. TITAN, thunderstorm identification, tracking, analysis, and nowcasting.

2.1. Process-Based Framework for Flood Frequency Analysis (FFA)

We estimate peak flow distributions using a process-based framework that combines realistic synthetic rainfall scenarios and distributed hydrologic modeling, hereafter the RainyDay- Hillslope-Link Model (HLM) framework. Previous efforts have used this approach to assess the importance of the level of detail in the spatial and temporal patterns of storms (Zhu et al., 2018) and climate-driven shifts in the seasonality of snowmelt and soil moisture (Yu et al., 2019) in peak flow distributions. Similarly, Perez, Mantilla, Krajewski, and Wright et al. (2019) used the RainyDay-HLM framework to examine the implications of sampling and model errors in RFFA.

2.1.1. Realistic Synthetic Rainfall Scenarios

The RainyDay software generates realistic synthetic storms via temporal resampling and spatial transposition of selected storms extracted from gridded data sets from a transposition domain A' that surrounds the watershed of interest. The selected storms are the largest noncontemporaneous rainfall events over A' , where the magnitude of each event is defined in terms of rainfall accumulation over a user-defined duration t and with the same size, shape, and orientation of the watershed of interest. The storms selected for stochastic storm transposition (SST) are called the “parent storms.” Based on a transposition domain A' bounded by latitudes 40.2°N and 45°N and longitudes 90.2°W and 96.7°W and using April–November Stage IV rainfall data for 2002–2018 (Du, 2011), we selected a total of 350 and 135 parent storms for TR and CR watersheds, respectively. Finally, following the approach proposed by Wright et al. (2017, 2020), we used RainyDay to generate 20 realizations of 500 synthetic annual rainfall scenarios for a total of 10,000 synthetic annual storms for each watershed (See the supporting information for a detailed description of the RainyDay procedure).

The direction, extent, and intensity of the parent storms were estimated using the thunderstorm identification, tracking, analysis, and nowcasting (TITAN) storm characterization algorithm (Dixon & Wiesner, 1993) and the object-based storm identification algorithm proposed by Davis et al. (2006) (Figure S3; Li et al., 2020). This analysis shows that the catalog of storms selected for the TR watershed exhibits a strong west-east directionality with an average direction $\bar{\alpha}_s = 92^\circ$ clockwise from the north (Figure 1b; similar results for CR watershed are not shown), consistent with the storm climatology in the region (Prein et al., 2020).

2.1.2. Distributed Hydrologic Modeling and Flood Frequency Analysis

We simulated the spectrum of extreme hydrologic response for each watershed by forcing the distributed hydrologic HLM with the 10,000 synthetic annual storms generated with RainyDay. HLM is a modular hydrologic model developed by the Iowa Flood Center (IFC) at the University of Iowa (Quintero et al., 2016, 2020) which decomposes the landscape into hillslopes and channels to represent a myriad of hydrologic processes including infiltration, overland flow, percolation, base flow, and channel routing. Here we use the HLM configuration currently implemented by the IFC for flood forecasting within Iowa to capture the flood dynamics in the region (Quintero et al., 2016). Continuous, long-term simulations from 2002 to 2018 using Stage IV radar rainfall data demonstrate the HLM’s ability to capture the flood dynamics for the study watersheds (Figure S4). The reader can find additional details about the assumptions behind the HLM and the specific configuration used in this study in the work of Quintero et al. (2016).

After verifying and validating the HLM for each watershed (Figure S4), we simulated the streamflow response for each of the 10,000 synthetic annual storms created with RainyDay. For each storm, we initialized the model using the procedure described by Yu et al. (2019), where initial soil moisture and baseflow conditions are randomly drawn from the long-term hydrologic simulations. This random selection was constrained to ensure the realistic “pairing” of rainstorms with seasonally consistent watershed conditions. We used a simulation period of 30 days to capture the peak in the hydrograph.

Finally, we derived nonparametric peak flow probability distributions from the simulated peak flows. The exceedance probability p for a single peak flow simulation within a distribution is calculated as $p = j / (1 + T_{\max})$, where j is the rank of the peak and T_{\max} is the number of storms in the distribution (i.e., 500 annual storms). Thus, this approach allows us to estimate exceedance probabilities as low as 0.002 (i.e., the 500-year recurrence interval). The 20 realizations of 500 storms allowed us to estimate 20 distinct peak flow distributions for each watershed, providing a measure of our estimates’ uncertainty.

2.2. Watershed Rotation in Process-Based Flood Frequency Analysis

The RainyDay-HLM framework was used to quantify the effect of storm direction in the peak flow probability distribution. To this end, we changed the direction of synthetic storms while preserving their other spatiotemporal characteristics (extent, duration, intensity, and velocity) and analyzed the resulting hydrographs. *Storm direction* is defined as the dominant direction of the moving rainstorm as it traverses the domain of interest, and it should not be confused with instantaneous fluctuations in the storm’s trajectory due to local

variability of the velocity field. Figures 1b and 1c illustrate the dominant storm trajectories and their statistics for the transposition domain used by RainyDay.

Changes in the storm direction were explored by systematically rotating the watershed clockwise by an angle θ about its centroid, equivalent to a counterclockwise rotation of the rainfall events. This rotation results in relative changes in the preferential direction of storm trajectories across the region ($\bar{\alpha}_s$) and the watershed orientation (α_w), defined as $\alpha = (\alpha_w + \theta) - \bar{\alpha}_s$. The relative change α is at the core of our analyses and interpretations. We repeat the storm identification, resampling, transposition, and subsequent hydrologic simulations for each rotation as described in Section 2.1. Example watershed rotations with the respective relative rotation α are shown in Figure 1d. We explored watershed rotations from 0° to 330° in steps of 30° for a total of 12 different rotations. With 10,000 events for each rotation, a total of 120,000 rainfall-runoff simulations were performed for each watershed.

3. Results and Discussion

3.1. Rotation Effects on Peak Flow Events

We begin by analyzing the effect of storm direction on specific rainfall-runoff events. This analysis provides a baseline to understand differences between sensitivity to storm direction in rainfall-runoff events and peak flow probability distributions. Three storms were selected at random for each watershed from the original parent storm catalog ($\theta = 0^\circ$) to illustrate the contrasting storm dynamics. To perform a fair comparison, where the watershed is forced by an equally extreme event in every direction, these storms were transposed for each watershed rotation to maximize the total watershed-average precipitation.

Spatial patterns of accumulated precipitation, calculated with the original rainfall data set, for the six selected events are shown in Figure S5. The precipitation amount depends on the watershed's size and orientation and the rainfall field's spatial structure as illustrated for each storm and different watershed rotations in Figures 2a and 2b. For instance, with a $\alpha = 18^\circ$ ($\theta = 0^\circ$) in the TR watershed, Event 1 produces an average of 195 mm over 72 h (the watershed's time of concentration); for the same event with a $\alpha = 78^\circ$ ($\theta = 60^\circ$), the watershed only receives an average of 140 mm. Differences in total rainfall amounts for the mesoscale CR watershed are lower. This observation can be explained by the larger size and longer accumulation period (12 days) which is more likely to encompass the storm core irrespective of the rotation angle.

We performed hydrologic simulations based on these six rainfall events and initialized the watershed with 100 different randomly sampled antecedent soil moisture conditions as explained in Section 2.1. The resulting hydrographs for rotations $\theta = 0^\circ$ and $\theta = 60^\circ$ with the three events are shown in Figure S6. For the TR watershed, the peak flow and total rainfall respond similar to the watershed rotation presenting the highest peak flows for storms traveling roughly in a downstream direction along the main channel ($\alpha = 18^\circ$; Figures 2a and 2c). In contrast, for the CR watershed, we found substantial differences in the effects of storm direction (i.e., watershed rotation) in the peak flow and total rainfall (Figures 2b and 2d). Specifically, the total rainfall presents limited variability as a function of rotation while the peak flow is highly sensitive. These results indicate that peak flows in larger watersheds are not necessarily maximized by storms traveling downstream along the main channel. It is also worth noting that the effect of storm direction in peak flows is not symmetric (Figure 2d), suggesting that the dynamic of runoff generation during extreme events is more complex in larger watersheds due to the variability in the rainfall positioning over the watershed.

3.2. Rotation Effects on Peak Flow Distributions

We focus on the peak flows (Q_{T_r}) with 25-, 100-, and 500-year recurrence intervals (T_r) as proxies for the peak flow probability distributions (Figures 3c and 3d). For each recurrence interval and storm direction, we quantify the variability of the Q_{T_r} estimates in terms of the 25th, 50th, and 75th quantiles from the 20 independent realizations of the RainyDay-HLM framework (shaded bands in Figures 3c and 3d).

Our results demonstrate that peak flow distributions at the scale of TR watershed or smaller are roughly independent of the storm direction. The symmetric nature of the rose diagrams for the TR watershed (Figure 3c) and four of its subwatersheds (Figure S7) support this conclusion. In contrast, for the larger CR

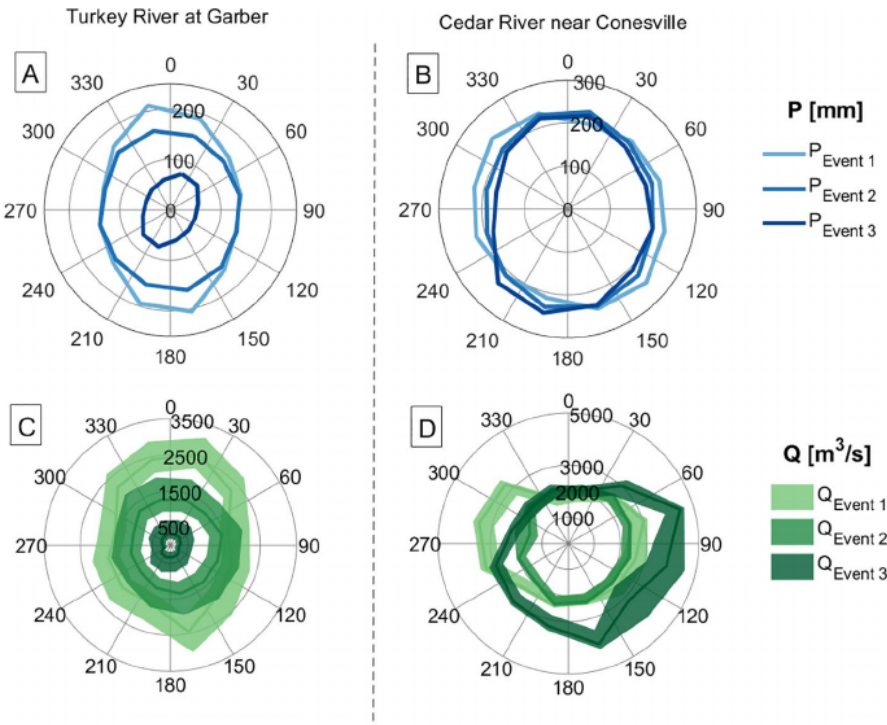


Figure 2. Total precipitation (Panels a and b) and peak flows (Panels c and d) for three specific rainfall-runoff events resulting from systematic watershed rotations from 0° to 330° , the angles are denoted by α . Total precipitation for the TR watershed and CR watershed was calculated over 72 h and 12 days, respectively. The green bands on the peak flows represent the interquartile range based on 100 different initial conditions. CR, Cedar River; TR, Turkey River.

watershed, the peak flows with 100- and 500-year return periods increase up to 25% for $\alpha = 103^\circ$ (a rotation of 60° ; Figure 3d). These results are consistent with the mean standard deviation and skewness of the peak flow simulations where significant variations are only observed for the CR watershed (Figure S8).

We compared the peak flow distributions calculated with the standard FFA (England, 2018) and RFFA (Eash et al., 2013) for the two watersheds (Figure 4). In general, the FFA estimated with the RainyDay-HLM framework under the current preferential storm direction ($\theta = 0^\circ$) is characterized by higher peak flow estimates than the standard FFA (referred to as B17C). This difference in peak flow estimates increases with the return period for the TR watershed and is relatively constant for the CR watershed. This finding can be explained by an ongoing period of elevated flood activity across the region over the last two decades when radar-based rainfall estimates are available and are consistent with previous FFA results using RainyDay in the TR watershed (Wright et al., 2017; Yu et al., 2019; Zhu et al., 2018).

The differences caused by changes in the preferential storm direction relative to the watershed orientation (mimicked by a watershed rotation here) are of particular interest. An $\alpha = 138^\circ$ ($\theta = 120^\circ$) results in minimal changes for the peak flow quantiles in the TR watershed (red and blue lines in Figure 4a). Similar results are found for other rotations of the TR watershed (not shown). In contrast, on highlighting the effect of scale, the peak flow quantiles show a drastic change, with differences increasing with the return period for a $\alpha = 103^\circ$ ($\theta = 60^\circ$) in the CR watershed (red and blue lines in Figure 4b); we selected this rotation because it displays the largest difference in peak flow quantiles between rotation angles. These results suggest a spatial scale between the TR watershed ($4,385 \text{ km}^2$) and the CR watershed ($20,168 \text{ km}^2$) for which changes in the storm direction substantially influence the distribution of peak flows.

We argue that the influence of storm direction (including the footprint of rainfall accumulation) in the mesoscale CR watershed, and lack thereof in the medium-scale TR watershed, is driven by differences in flood mechanistic processes that depend on the interplay between storm scale and watershed size. For instance, the typical characteristic area for the parent storms is approximately $1,680 \text{ km}^2$ with a range

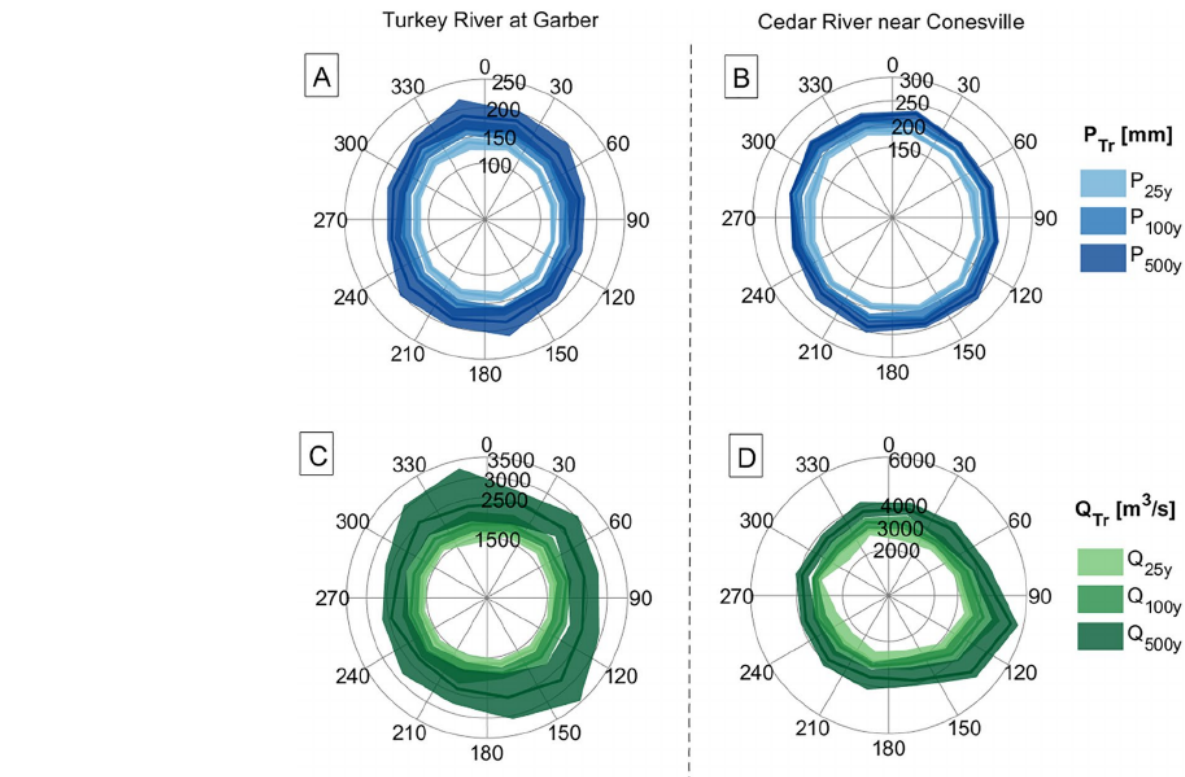


Figure 3. Total precipitation (Panels a and b) and peak flows (Panels c and d) for 25-, 100-, and 500-year recurrence intervals associated with rotations from 0° to 330° , the angles are denoted by α . Green and blue bands represent the interquartile range based on 20 independent realizations of the RainyDay-HLM framework. HLM, Hillslope-Link Model.

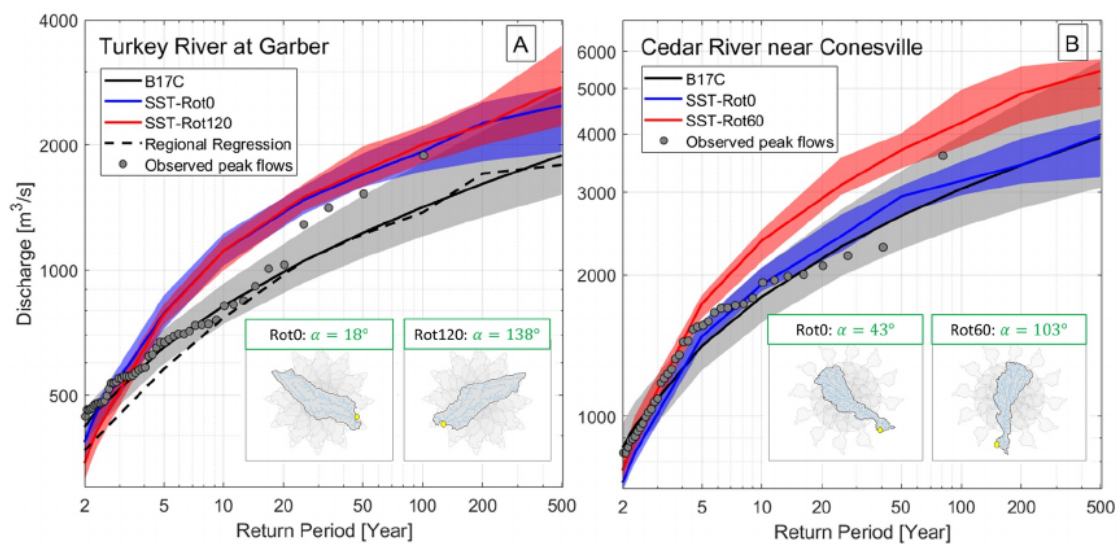


Figure 4. Peak flow quantiles estimated from Bulletin 17C (England, 2018), regional regression equations (Eash, 2015), observed peak flows, and RainyDay HLM with (a) $\theta = 0^\circ$ Rotation (SST-Rot0) and $\theta = 120^\circ$ Rotation (SST-Rot120) for TR watershed and (b) $\theta = 60^\circ$ Rotation (SST-Rot60) for CR watershed. The regional regression for the CR watershed does not exist due to the large watershed size. CR, Cedar River; HLM, Hillslope-Link Model; SST, stochastic storm transposition; TR, Turkey River.

of 227 to 13,000 km² (see the distribution of hourly estimates of storm area in Figure S3). The area of the TR watershed is 4,385 km² ($A_{\text{watershed}} / \overline{A_{\text{storm}}} \sim 2.6$), and the area of the CR watershed is 20,168 km² ($A_{\text{watershed}} / \overline{A_{\text{storm}}} \sim 12$). The size of the storms driving runoff generation in the TR watershed is in the order of the size of the watershed, leading to a similar distribution of rainfall fluxes for different rotations. In contrast, the CR watershed is large when compared to the average storm scale (about 12 times larger), and therefore the rotation results in the runoff activation of different parts of the landscape with a marked effect in the peak flow distribution. This argument is supported by the rainfall patterns of the five highest peak flows for the TR and CR watersheds with rotations of $\theta = 0^\circ$ and $\theta = 60^\circ$ (see [videos](#) in the supporting information). In this case, the rainfall patterns are nearly invariant for $\theta = 0^\circ$ and $\theta = 60^\circ$ in the TR watershed. The patterns for the CR watershed show a more dynamic and heterogeneous behavior; for instance, the highest peak flow in the simulations for the CR watershed with $\theta = 60^\circ$ is generated by the compounding effect of an initial storm located in the upper part of the watershed followed by a second storm at the lower part, a behavior absent for $\theta = 0^\circ$.

3.3. Potential Implications Under Future Shifts in the Preferential Storm Direction

The mesoscale CR watershed results suggest that watersheds in the study region with $\alpha \in [60^\circ, 150^\circ]$ (See Figure 3d) are the most vulnerable to extreme changes in peak flow distributions due to changes in preferential storm directions. For instance, a shift of α from 73° to 103° equivalent to a counterclockwise change of 30° in the preferential storm direction could increase the 100-year flood by $\sim 20\%$ (Figure 3d). These results could be considered as an initial approximation to understand how sensitive the neighboring watersheds are to changes in peak flows by variations in $\bar{\alpha}_s$ (See Figure S2 for an example showing the variability of α at a regional scale). Nonetheless, further analysis considering different watersheds under contrasting climatological conditions is needed to understand the impacts in a larger spectrum of watershed geometries in tandem with different storm sizes.

4. Conclusions

Using realistic storm scenarios, we found that the role of the preferential storm direction on rainfall-runoff events strongly depends on the characteristic scale of the rainfall events relative to the watershed's size, with the sensitivity increasing for smaller storms. In particular, peak flow probability distributions are independent of storm direction at the spatial scale of the TR watershed (4,385 km²) and a series of its subwatersheds. In contrast, the peak flow probability distribution for the mesoscale CR watershed (20,168 km²) is significantly affected by storm direction, showing an increase in peak flow quantiles of up to 25%.

These findings provide a critical step toward a deeper understanding of the potential implications of future shifts in storm directions under a changing climate. In particular, it sets expectations for changes in flood frequency statistics and highlights the limitations of regionalization techniques. RFFA efforts that neglect storm direction are liable to greatly misrepresent the actual flood behavior in certain watersheds, particularly those that are relatively large or whose geometry differs substantially from the prevailing watershed orientation in the region. Meanwhile, high-resolution regional climate model projections should be assessed for changes in the simulated storm direction.

Acknowledgments

This work was funded by the U.S. Department of Energy's Office of Biological and Environmental Research, Subsurface Biogeochemical Research Program Scientific Focus Area at the Pacific Northwest National Laboratory, and the National Science Foundation awards 1830172 and 2020814. D. B. Wright's contributions were supported by the U.S. National Science Foundation Hydrologic Sciences Program CAREER project EAR-1749638. The Iowa Flood Center supported R. Mantilla's contributions.

Data Availability Statement

Documentation and codes of HLM are available at <https://asynch.readthedocs.io/en/latest/> and <https://github.com/Iowa-Flood-Center/asynch>. The RainyDay software is available at <https://github.com/danielb-wright/RainyDay2>. The peak flow values generated from the RainyDay-HLM framework for the TR and CR watersheds can be downloaded from https://github.com/gjperez/GRL_Peak_Flows_Rotations.

References

Ayalew, T. B., & Krajewski, W. F. (2017). Effect of river network geometry on flood frequency. *A Tale of Two Watersheds in Iowa*, 22(8), 1–7. [https://doi.org/10.1061/\(ASCE\)HE.1943-5584.0001544](https://doi.org/10.1061/(ASCE)HE.1943-5584.0001544)

Chang, C.-L. (2007). Influence of moving rainstorms on watershed responses. *Environmental Engineering Science*, 24(10), 1353–1360. <https://doi.org/10.1089/ees.2006.0220>

Chang, W., Stein, M. L., Wang, J., Kotamarthi, V. R., & Moyer, E. J. (2016). Changes in spatiotemporal precipitation patterns in changing climate conditions. *Journal of Climate*, 29(23), 8355–8376. <https://doi.org/10.1175/JCLI-D-15-0844.1>

Cheng, L., & AghaKouchak, A. (2015). Nonstationary Precipitation Intensity-Duration-Frequency Curves for Infrastructure Design in a Changing Climate. *Scientific Reports*, 4(1), 1–6. <https://doi.org/10.1038/srep07093>

Davis, C., Brown, B., & Bullock, R. (2006). Object-based verification of precipitation forecasts. Part II: Application to convective rain systems. *Monthly Weather Review*, 134(7), 1785–1795. <https://doi.org/10.1175/MWR3146.1>

Dawdy, D. R., Griffis, V. W., & Gupta, V. K. (2012). Regional flood-frequency analysis: How we got here and where we are going. *Journal of Hydrologic Engineering*, 17(9), 953–959. [https://doi.org/10.1061/\(ASCE\)HE.1943-5584.0000584](https://doi.org/10.1061/(ASCE)HE.1943-5584.0000584)

de Lima, J. L. M. P., & Singh, V. P. (2003). Laboratory experiments on the influence of storm movement on overland flow. *Physics and Chemistry of the Earth, Parts A/B/C*, 28(6–7), 277–282. [https://doi.org/10.1016/S1474-7065\(03\)00038-X](https://doi.org/10.1016/S1474-7065(03)00038-X)

Dixon, M., & Wiener, G. (1993). TITAN: Thunderstorm identification, tracking, analysis, and nowcasting – a radar-based methodology. *Journal of Atmospheric and Oceanic Technology*, 10(6), 785–797. [https://doi.org/10.1175/1520-0426\(1993\)010<0785:TTITAA>2.0.CO;2](https://doi.org/10.1175/1520-0426(1993)010<0785:TTITAA>2.0.CO;2)

Du, J. (2011). GCIP/EOP surface: Precipitation NCEP/EMC 4KM gridded data (GRIB) stage IV data version 1.0. UCAR/NCAR – Earth Observing Laboratory. <https://doi.org/10.5065/D6PG1QDD>

Eash, D. A. (2015). Comparisons of estimates of annual exceedance-probability discharges for small drainage basins in Iowa, based on data through water year 2013. <https://doi.org/10.3133/sir20155055>

Eash, D. A., Barnes, K. K., & Veilleux, A. G. (2013). Methods for estimating annual exceedance-probability discharges for streams in Iowa, based on data through water year 2010 scientific investigations report 2013 – 5086. <https://doi.org/10.3133/sir20135086>

England, J. F. (2018). Guidelines for determining flood flow frequency Bulletin 17C book 4, hydrologic analysis and interpretation techniques and methods 4-B5. Retrieved from <https://pubs.usgs.gov/tm/04/b05/tm4b5.pdf>

Fang, Z. N., Shultz, M. J., Wienhold, K. J., Zhang, J., & Gao, S. (2019). Case study: Comparative analysis of hydrologic simulations with areal-averaging of moving rainfall. *Hydrology*, 6(1), 12. <https://doi.org/10.3390/hydrology6010012>

Furey, P. R., Troutman, B. M., Gupta, V. K., Krajewski, W. F., & Asce, M. (2016). Connecting event-based scaling of flood peaks to regional flood frequency relationships. *Journal of Hydrologic Engineering*, 21(10), 1–11. [https://doi.org/10.1061/\(ASCE\)HE.1943-5584.0001411](https://doi.org/10.1061/(ASCE)HE.1943-5584.0001411)

Gao, S., & Fang, Z. N. (2019). Investigating hydrologic responses to spatio-temporal characteristics of storms using a Dynamic Moving Storm generator. *Hydrological Processes*, 33(21), 2729–2744. <https://doi.org/10.1002/hyp.13524>

Goodwell, A. E. (2020). "It's Raining Bits": Patterns in directional precipitation persistence across the United States. *Journal of Hydrometeorology*, 21(12), 2907–2921. <https://doi.org/10.1175/JHM-D-20-0134.1>

Hamed, K., & Rao, A. R. (2019). *Flood frequency analysis*. CRC press.

Han, K.-Y., Jeon, M.-W., & Choi, K.-H. (2004). Runoff analysis due to the moving storm. *Journal of Korea Water Resources Association*, 37, 823–836. <https://doi.org/10.3741/jkwa.2004.37.10.823>

Hansli, E. (2012). Possible impacts of floods and droughts on water quality. *Journal of Hydro-environment Research*, 6, 145–150. <https://doi.org/10.1016/j.jher.2012.01.008>

Hirabayashi, Y., Mahendran, R., Koitala, S., Konoshima, L., Yamazaki, D., Watanabe, S., et al. (2013). Global flood risk under climate change. *Nature Climate Change*, 3(9), 816–821. <https://doi.org/10.1038/nclimate1911>

Hosking, J. R. M., & Wallis, J. R. (1993). Some statistics useful in regional frequency analysis. *Water Resources Research*, 29(92). <https://doi.org/10.1029/92wr01980>

Kim, D.-H., & Seo, Y. (2013). Hydrodynamic analysis of storm movement effects on runoff hydrographs and loop-rating curves of a V-shaped watershed. *Water Resources Research*, 49(10), 6613–6623. <https://doi.org/10.1002/wrcr.20535>

Lee, T., Shin, J., Park, T., & Lee, D. (2015). Basin rotation method for analyzing the directional influence of moving storms on basin response. *Stochastic Environmental Research and Risk Assessment*, 29(1), 251–263. <https://doi.org/10.1007/s00477-014-0870-y>

Li, Z., Wright, D. B., Zhang, S. Q., Kirschbaum, D. B., & Hartke, S. H. (2020). Object-based comparison of data-driven and physics-driven satellite estimates of extreme rainfall. *Journal of Hydrometeorology*, 21(12), 2759–2776. <https://doi.org/10.1175/JHM-D-20-0041.1>

Marco, J. B., & Valdés, J. B. (1998). Partial area coverage distribution for flood frequency analysis in arid regions. *Water Resources Research*, 34(9), 2309–2317. <https://doi.org/10.1029/98WR01246>

Mbengue, C., & Schneider, T. (2013). Storm track shifts under climate change: What can be learned from large-scale dry dynamics. *Journal of Climate*, 26(24), 9923–9930. <https://doi.org/10.1175/JCLI-D-13-00404.1>

Milly, P. C. D., Betancur, J., Falkenmark, M., Hirsch, R. M., Kundzewicz, Z. W., Lettenmaier, D. P., et al. (2014). On critiques of "stationarity is dead: Whither water management?" *Water Resources Research*, 50, 1823–1839. <https://doi.org/10.1002/2013WR014722>

Nunes, J. P., de Lima, J. L. M. P., Singh, V. P., de Lima, M. I. P., & Vieira, G. N. (2006). Numerical modeling of surface runoff and erosion due to moving rainstorms at the drainage basin scale. *Journal of Hydrology*, 330(3–4), 709–720. <https://doi.org/10.1016/j.jhydrol.2006.04.037>

Perez, G., Mantilla, R., & Krajewski, W. F. (2018a). The influence of spatial variability of width functions on regional peak flow regressions. *Water Resources Research*, 54(10), 7651–7669. <https://doi.org/10.1029/2018WR023509>

Perez, G., Mantilla, R., & Krajewski, W. F. (2018b). Spatial patterns of peak flow quantiles based on power-law scaling in the Mississippi River Basin. In A. A. Tsionis (Ed.), *Advances in Nonlinear Geosciences* (pp. 497–518). Springer International Publishing. https://doi.org/10.1007/978-3-319-58895-7_23

Perez, G., Mantilla, R., Krajewski, W. F., & Quintero, F. (2019). Examining observed rainfall, soil moisture, and river network variabilities on peak flow scaling of rainfall-runoff events with implications on regionalization of peak flow quantiles. *Water Resources Research*, 55(12), 10707–10726. <https://doi.org/10.1029/2019WR026028>

Perez, G., Mantilla, R., Krajewski, W. F., & Wright, D. B. (2019). Using physically based synthetic peak flows to assess local and regional flood frequency analysis methods. *Water Resources Research*, 55(11), 8384–8403. <https://doi.org/10.1029/2019WR024827>

Prein, A. F., Liu, C., Ikeda, K., Bullock, R., Rasmussen, R. M., Holland, G. J., & Clark, M. (2020). Simulating North American mesoscale convective systems with a convection-permitting climate model. *Climate Dynamics*, 55(0), 95–110. <https://doi.org/10.1007/s00382-017-3993-2>

Quintero, F., Krajewski, W. F., Mantilla, R., Small, S., & Seo, B.-C. (2016). A Spatial-dynamical framework for evaluation of satellite rainfall products for flood prediction. *Journal of Hydrometeorology*, 17(8), 2137–2154. <https://doi.org/10.1175/JHM-D-15-0195.1>

Quintero, F., Krajewski, W. F., Seo, B.-C., & Mantilla, R. (2020). Improvement and evaluation of the Iowa Flood Center Hillslope Link Model (HLM) by calibration-free approach. *Journal of Hydrology*, 584, 124686. <https://doi.org/10.1016/j.jhydrol.2020.124686>

Seo, Y., & Schmidt, A. R. (2013). Network configuration and hydrograph sensitivity to storm kinematics. *Water Resources Research*, 49(4), 1812–1827. <https://doi.org/10.1002/wrcr.20115>

Seo, Y., & Schmidt, A. R. (2014). Evaluation of drainage networks under moving storms utilizing the equivalent stationary storms. *Natural Hazards*, 70(1), 803–819. <https://doi.org/10.1007/s11069-013-0845-1>

Sigaroodi, S. K., & Chen, Q. (2016). Effects and consideration of storm movement in rainfall-runoff modeling at the basin scale. *Hydrology and Earth System Sciences*, 20(12), 5063–5071. <https://doi.org/10.5194/hess-20-5063-2016>

Singh, V. P. (2005). Effects of storm direction and duration on infiltrating planar flow with partial coverage. *Hydrological Processes*, 19(4), 969–992. <https://doi.org/10.1002/hyp.5554>

Stedinger, J. R., & Griffis, V. W. (2008). Flood frequency analysis in the United States: Time to update. *Journal of Hydrologic Engineering*, 13(4), 199–204. [https://doi.org/10.1061/\(ASCE\)1084-0699\(2008\)13:4\(199\)](https://doi.org/10.1061/(ASCE)1084-0699(2008)13:4(199))

Tamarin-Brodsky, T., & Kaspi, Y. (2017). Enhanced poleward propagation of storms under climate change. *Nature Geoscience*, 10(12), 908–913. <https://doi.org/10.1038/s41561-017-0001-8>

ten Veldhuis, M.-C., Zhou, Z., Yang, L., Liu, S., & Smith, J. (2017). The role of storm dynamics and scale in controlling urban flood response. *Hydrology and Earth System Sciences Discussions*, 1–28. <https://doi.org/10.5194/hess-2017-197>

Volpi, E., Di Lazzaro, M., & Fiori, A. (2013). Analytical modeling of the hydrologic response under moving rainstorms: Storm-catchment interaction and resonance. *Journal of Hydrology*, 493, 132–139. <https://doi.org/10.1016/j.jhydrol.2013.04.025>

Wright, D. B., Mantilla, R., & Peters-Lidard, C. D. (2017). A remote sensing-based tool for assessing rainfall-driven hazards. *Environmental Modelling & Software*, 90, 34–54. <https://doi.org/10.1016/j.envsoft.2016.12.006>

Wright, D. B., Yu, G., & England, J. F. (2020). Six decades of rainfall and flood frequency analysis using stochastic storm transposition: Review, progress, and prospects. *Journal of Hydrology*, 585, 124816. <https://doi.org/10.1016/j.jhydrol.2020.124816>

Yu, G., Wright, D. B., Zhu, Z., Smith, C., & Holman, K. D. (2019). Process-based flood frequency analysis in an agricultural watershed exhibiting nonstationary flood seasonality. *Hydrology and Earth System Sciences*, 23(5), 2225–2243. <https://doi.org/10.5194/hess-23-2225-2019>

Zhu, Z., Wright, D. B., & Yu, G. (2018). The impact of rainfall space-time structure in flood frequency analysis. *Water Resources Research*, 54(11), 8983–8998. <https://doi.org/10.1029/2018WR023550>

References From the Supporting Information

Ayalew, T. B., Krajewski, W. F., & Mantilla, R. (2015). Analyzing the effects of excess rainfall properties on the scaling structure of peak discharges: Insights from a mesoscale river basin. *Water Resources Research*, 51, 3900–3921. <https://doi.org/10.1002/2014WR016258>

Beven, K. J. (2020). A history of the concept of time of concentration. *Hydrology and Earth System Sciences Discussions*, 1–28. <https://doi.org/10.5194/hess-2019-588>

Dingman, S. L. (2008). *Physical hydrology*. University of Simon Fraser Library. Retrieved from <https://books.google.com/books?id=Gi1KwwEACAAJ>

Smith, J. a., Baeck, M. L., Villarini, G., Wright, D. B., & Krajewski, W. (2013). Extreme flood response: The June 2008 flooding in Iowa. *Journal of Hydrometeorology*, 14(6), 1810–1825. <https://doi.org/10.1175/JHM-D-12-0191.1>